

Plausible megathrust tsunamis in the eastern Mediterranean Sea

Brett L. Valle PhD

Senior Engineer, Bechtel National, Geotechnical & Hydraulic Engineering Services (G&HES), San Francisco, CA, USA

Nikos Kalligeris MSc

PhD Student, Department of Civil and Environmental Engineering, University of Southern California, Los Angeles, CA, USA

Angelos N. Findikakis PhD, PE

Senior Principal Engineer, Bechtel National, Geotechnical & Hydraulic Engineering Services (G&HES), San Francisco, CA, USA

Emile A. Okal PhD

Professor, Department of Earth & Planetary Sciences, Northwestern University, Evanston, IL, USA

Lavinia Melilla PhD, CEng, MICE

Port Area Manager, Bechtel Civil, London, UK

Costas E. Synolakis PhD

Professor, Department of Civil and Environmental Engineering, University of Southern California, Los Angeles, CA, USA

Tsunamis have occurred at rates of about one to two per century in the Mediterranean Sea, on average, over the past 2000 years. However, most of these events have been of small amplitude and quantification of tsunami hazards in the eastern Mediterranean Sea remains difficult. Simulations were performed for a series of plausible $M_w \geq 8$ seismic events originating along the Hellenic subduction zone and NW Cyprian Arc. Their locations and source characteristics represent events that are similar to the largest historical events, including the AD 365 and AD 1303 events, and in consideration of potential future events. The hydrodynamic simulations used the numerical model are known as the method of splitting tsunami (Most). Reported results include simulated wave amplitudes in the eastern Mediterranean Sea, specifically in the western Nile Delta region near the Rosetta promontory and Egypt's largest coastal city, Alexandria.

1. Introduction

The Hellenic subduction zone is an active tectonic feature of the eastern Mediterranean Sea and represents the subduction of the Nubia (Africa) plate beneath the Aegean (McClusky *et al.*, 2000) (Figure 1). Previous studies have established that the Hellenic subduction zone may represent a modern-day tsunami hazard (Shaw *et al.*, 2008; UNU-EHS *et al.*, 2009). However, most tsunami events generated along this zone have been of small amplitude, with significantly damaging tsunamis documented in the historical record occurring on a much less frequent basis. This frequency makes their study and quantification difficult, especially in the eastern Mediterranean Sea, where recurrence times for large earthquakes are estimated to be of the order of several centuries. For example, over the last 2000 years, the historical record contains only two earthquakes of $M_w \geq 8$ (Shaw and Jackson, 2010). As discussed by Shaw and Jackson (2010), rare large events are thought to occur along steeply dipping splay faults located off the main subduction interface. These splay faults have been inferred to account for 5–15% of the Nubia–Aegean convergence, with the remaining convergence (85–95%) believed to be accommodated by aseismic slip, with small local patches slipping in earthquakes of up to about $M_w = 6.0$ (Shaw and Jackson, 2010).

Historical tsunamigenic earthquakes in the eastern Mediterranean have been described in several works (e.g. Ambraseys and Synolakis, 2010; Salamon *et al.*, 2007; Shaw *et al.*, 2008). Most notable among these events are those on 21 July AD 365, most likely located southwest of Crete, on a shallow-dipping thrust fault near the Hellenic Trench, and whose tsunami inundated

coastal sites in North Africa, the Adriatic, Greece and Sicily, and on 8 August AD 1303, estimated to have occurred near Rhodes, also causing widespread damage in the eastern Mediterranean (Shaw *et al.*, 2008). Based on partitioning of the seismic and aseismic convergence observed for the AD 365 event in SW Crete to the entire Hellenic subduction zone, Shaw *et al.* (2008) estimated that an event similar to the AD 365 event may occur about every 800 years, with the last event occurring in AD 1303 (Ambraseys and Synolakis, 2010), indicating that the area may be ripe for a new major event.

Located to the east of the Hellenic subduction zone, the Cyprian Arc forms the plate boundary between the Anatolian plate in the north and the Nubian and Sinai plates in the south (Wdowinski *et al.*, 2006) (Figure 1). As discussed by Wdowinski *et al.* (2006), the Cyprian Arc is subjected to subduction, collision and transcurrent tectonic processes. Although the Cyprian Arc has experienced little seismicity over the last century (Wdowinski *et al.*, 2006), it is also a source of tsunamigenic earthquakes. The largest tsunamigenic event along the Cyprian Arc occurred on 11 May AD 1222, destroying the city of Paphos (Yolsal *et al.*, 2007). The likelihood of future tsunamigenic events along the Cyprian Arc is not well established.

The purpose of this study was to analyse plausible 'worst-case' megathrust ($M_w \geq 8$) tsunamigenic events that could occur along the Hellenic and Cyprian Arcs, and which may impact the western Nile Delta region near the Rosetta promontory and Egypt's largest coastal city, Alexandria. The magnitude of the analysed events was

Offprint provided courtesy of www.icevirtuallibrary.com
 Author copy for personal use, not for distribution

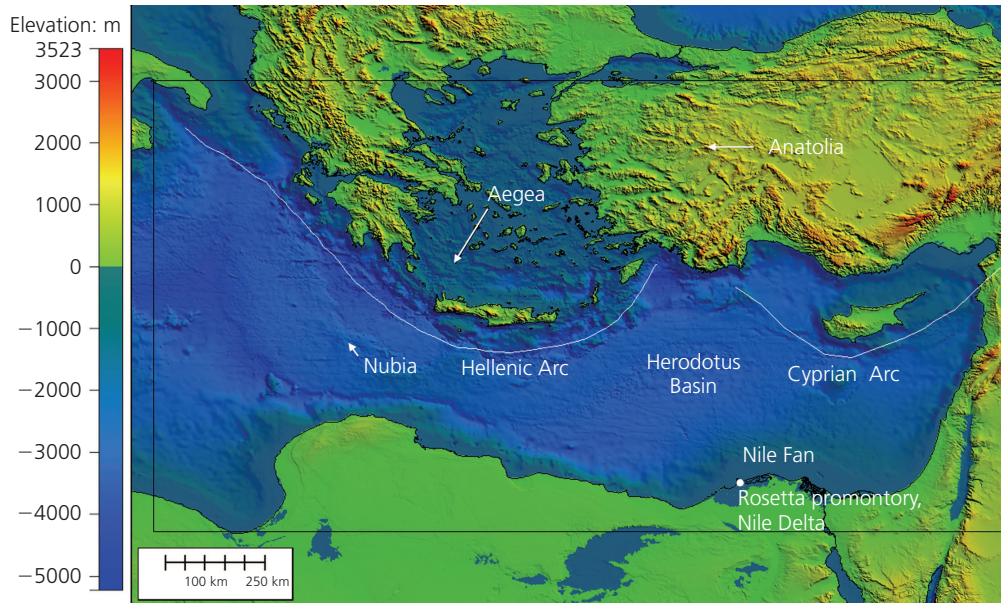


Figure 1. Simplified tectonic setting of the eastern Mediterranean region (Ebeling *et al.*, 2012; IOC *et al.*, 2003)

based on consideration of segments of the Hellenic and Cyprian Arcs that could plausibly rupture. The locations and source characteristics represent events that are similar to the largest historical events, and in consideration of potential future events.

2. Tsunami simulation method

Tsunami simulations were performed using the numerical model known as the method of splitting tsunami (Most) (Flouri *et al.*,

2013; PMEL, 2006; Synolakis, 2004; Titov and Synolakis, 1998). Most has been validated and verified extensively using benchmark experiments and field data (Liu *et al.*, 2008; NTHMP, 2012; Synolakis *et al.*, 2008). In Most, tsunami evolution is simulated in three phases: generation, propagation and inundation.

- The generation phase uses the formalism proposed by Okada (1985) to compute static deformation of the ocean floor

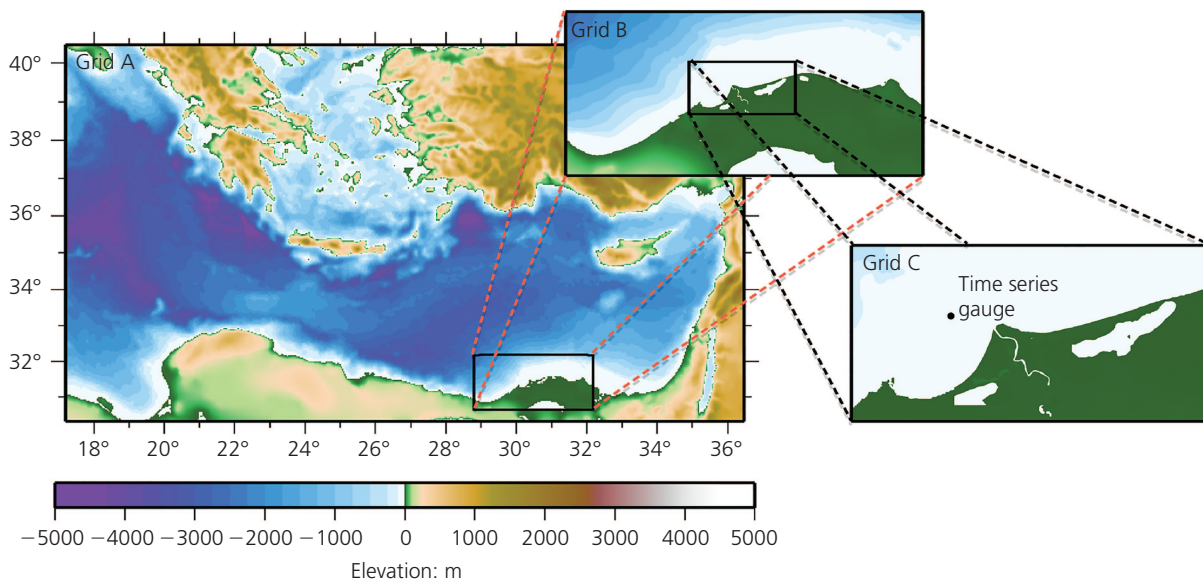


Figure 2. Model grids A, B and C used for tsunami simulations in the eastern Mediterranean Sea

Offprint provided courtesy of www.icevirtuallibrary.com
Author copy for personal use, not for distribution

resulting from a finite dislocation representing an earthquake source (Titov and González, 1997).

- The second phase propagates the generated tsunami across the ocean by solving the depth-integrated non-linear shallow water (NLSW) equations in two spatial dimensions and in time. The numerical solution of these equations uses a finite-difference algorithm that splits the NLSW equations into a pair of systems.
- The inundation phase simulates the shallow water behaviour of a tsunami by extending the solution of the NLSW equations on land using a moving-boundary scheme to estimate tsunami runup onto dry land (Titov and Synolakis, 1998).

The bathymetry of the eastern Mediterranean included in the modelling was obtained from GEBCO-08 grid, a global 30 arc second grid of publicly available bathymetric data, downloaded from the website of the general bathymetric chart of the oceans (GEBCO) (IOC *et al.*, 2003). The GEBCO-08 grid was generated by combining quality-controlled ship depth soundings with interpolations between sounding points. While the bathymetry data are relatively coarse, the resolution of the GEBCO data is considered to be sufficient for the modelling analysis at larger depths. Additional high-resolution bathymetry data for the western Nile Delta were also incorporated in the model.

Three nested grids were used in the analysis (Figure 2). As shown in Table 1, the resolutions of grids A, B and C are 0.0292 arc degrees (≈ 3000 m), 0.004867 arc degrees (≈ 500 m) and 0.00081 arc degrees (≈ 84 m) respectively. The grid resolutions are consistent with the recommendations of the Pacific Marine Environmental Laboratory (PMEL, 2006). The progressively higher resolution in the area of interest, from grid A to grid B to grid C (Figure 2), ensures sufficient numerical resolution of non-linear effects as the wave moves from deep water towards the shoreline. The finest resolution grid (grid C) covers the area of the western Nile Delta near the Rosetta promontory, including the area east of Alexandria, Egypt.

3. Megathrust tsunami sources in the eastern Mediterranean Sea

Four plausible megathrust tsunami source events were considered in the analysis (Table 2). Sources S1, S2 and S3 were located along the Hellenic subduction zone and source S4 was located

Grid	Description	Grid resolution	Number of grid nodes (longitude \times latitude)
A	Coarse	$\Delta x = \Delta y = 0.0292^\circ (\approx 3000 \text{ m})$	661 \times 349 nodes
B	Intermediate	$\Delta x = \Delta y = 0.004867^\circ (\approx 500 \text{ m})$	697 \times 319 nodes
C	Fine	$\Delta x = \Delta y = 0.00081^\circ (\approx 84 \text{ m})$	1249 \times 613 nodes

Table 1. Spatial resolution of model grids used in the simulations

	Scenario			
	S1 ^a	S2 ^b	S3	S4
Magnitude M_w	8.4	8.4	8.5	8.4
Length: km	100	190	240 ^c	200 ^d
Width: km	90	90	100 ^c	100 ^d
Dip: degrees	30	20	20	20
Rake: degrees	90	90	90	90
Strike: degrees	315	235	235	315
Slip: m	20	10	7.5–15 ^c	5–11 ^d
Depth: km	0 ^e	7.5	7.5	10

^a Source S1 adapted from Shaw *et al.* (2008) (see Figure 3(a)).

^b Source S2 adapted from source parameters reported by Mitsoudis *et al.* (2012) (see Figure 3(b)).

^c Source parameters included six fault segments, with an area of 80 km \times 50 km for each segment (see Figure 3(c)). A 15 m slip was assumed in the central third of the rupture planes and a 7.5 m slip in the outer planes.

^d Source parameters included eight fault segments, with an area of 50 km \times 50 km for each segment (see Figure 3(d)). Table 1 of Wdowinski *et al.* (2006) was used to define the source. An 11 m slip was assumed in the four central planes and a 5 m slip in the four outer planes.

^e S1 depth refers to the depth of the up-dip edge of the fault plane.

Table 2. Seismic parameters of sources used in the simulations

along the NW Cyprian Arc. In the case of S1, a detailed description of the earthquake source has been reported by Shaw *et al.* (2008) and its parameters were directly input into the algorithm proposed by Okada (1985) (Figure 3(a)). The earthquake of 21 July AD 365 is the only event for which we have historical data, field observations and radiocarbon data (Ambraseys and Synolakis, 2010). Historical reports for other events have not yet been correlated with field geologic studies or modelling for other major tsunamigenic events in the eastern Mediterranean (Ambraseys and Synolakis, 2010). For S2, S3 and S4, only a general estimate of the size of historical events is available and thus scaling laws were used (Geller, 1976) to derive appropriate parameters for the seismic sources. The tacit assumption behind this approach (i.e. that the largest earthquakes in the study area follow seismic similitude) may be legitimately questioned since several major earthquakes, such as that in Tohoku in 2011 (Ammon *et al.*, 2011; Fujii *et al.*, 2011; Pollitz *et al.*, 2011)

Offprint provided courtesy of www.icevirtuallibrary.com
Author copy for personal use, not for distribution

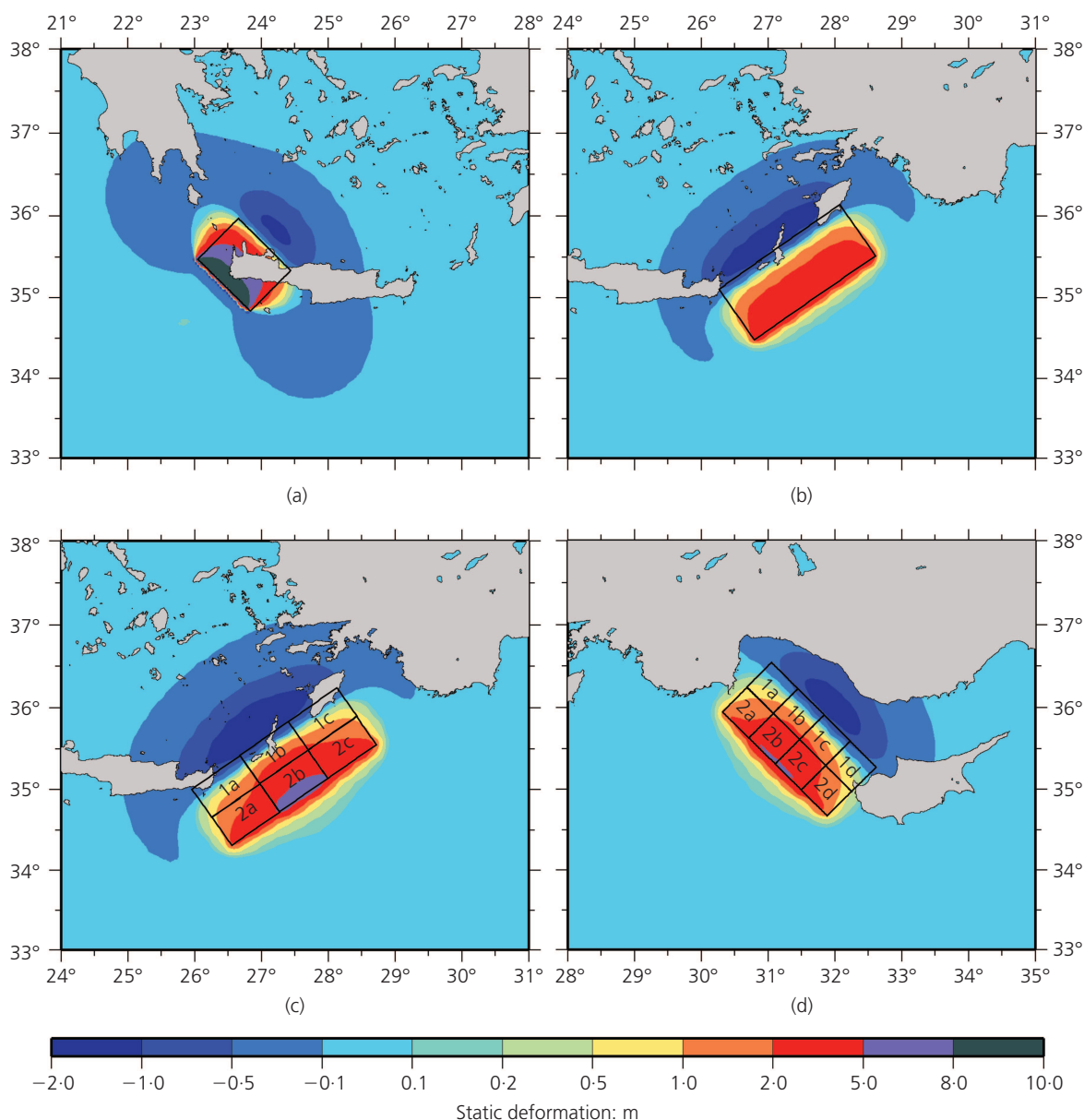


Figure 3. Initial conditions (wave elevation) for sources (a) S1, (b) S2, (c) S3 and (d) S4; source parameters for the fault planes are provided in Table 2

and the Cretan event of AD 365 as modelled by Shaw *et al.* (2008) and Flouri *et al.* (2013), deviate from the scaling laws. Nevertheless, this approach was used for the simulations as it is the only method available in the absence of detailed geological work regarding historical sources.

In this context, the parameters for S2 are based on those published by Mitsoudis *et al.* (2012), but with a larger slip, equal to 10 m over a 190 km segment of the eastern Hellenic Arc (Figure 3(b)). The location of source S2 is also different from that analysed by Mitsoudis *et al.* (2012), and was

selected to produce the maximum potential runup along the western Nile Delta region near the Rosetta promontory. In the framework of probable subduction along the entire eastern segment of the Hellenic Arc, the location of S2 is different in this study from that analysed by Mitsoudis *et al.* (2012), as Mitsoudis *et al.* (2012) investigated a worst-case scenario for the island of Rhodes. The present study is concerned with tsunami effects at a more distant range, along the western Nile Delta region near the Rosetta promontory, for which source S2 is a worst-case scenario rupturing the entire tectonic segment.

Offprint provided courtesy of www.icevirtuallibrary.com
Author copy for personal use, not for distribution

The source parameters for S3 were similar to S2, with the addition of a variable-slip source mechanism with six fault planes (Figure 3(c)). Instead of the uniform 10 m slip assumed in S2, in S3 it was assumed that the central third of the rupture planes slips by 15 m and its outer planes by 7.5 m. This event corresponds to an earthquake with a moment magnitude 8.5.

Along the Cyprian Arc, source S4 is derived from the study reported by Wdowinski *et al.* (2006). While seismicity is documented along the short southwestern coast of Cyprus and the longer southeastern Cyprus–Larnaca Ridge system, the model of Wdowinski *et al.* (2006) shows convergence with significantly more normal azimuths and faster rates along the northwestern part of the Cyprian Arc. Source S4 was therefore placed along the NW Cyprian Arc. As in the case of S3, source S4 involves a composite mechanism featuring eight fault segments (Figure 3(d)). An 11 m slip was assumed in the four central planes and a 5 m slip in the four outer planes. As with the AD 365 source (S1) described by Shaw *et al.* (2008), the area and displacement of the maximum-slip fault patches for the variable-slip sources (S3 and S4) are larger than typically observed in most large earthquake sources (Scholz *et al.*, 1986). However, sources S3 and S4 are inspired by and comparable to one of the maximum-slip fault patches in the Sumatra earthquake of 2004 (Subarya *et al.*, 2006).

4. Tsunami simulation results

Results from the simulations are presented in Figures 4 to 8. For S1 (a $M_w = 8.4$ model of the AD 365 event SW of Crete), a strong lobe of directivity is aimed at the coast of Cyrenaica, Libya (Ben-Menahem and Rosenman, 1972), while a secondary lobe, presumably controlled by shallower bathymetry, is aimed towards the Peloponnese in Greece (Figure 4). Tsunami wave interaction with shallow bathymetry also sustains maximum amplitudes (zero-to-peak) in the 2–3 m range along the eastern

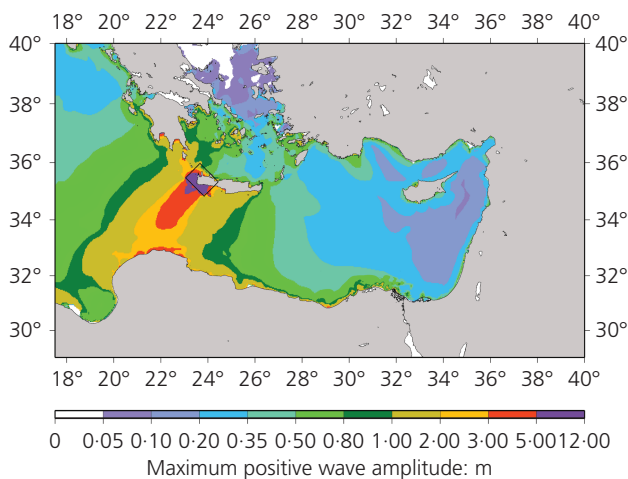


Figure 4. Maximum simulated tsunami amplitude for S1 ($M_w = 8.4$ and AD 365-like event) in the eastern Mediterranean Sea

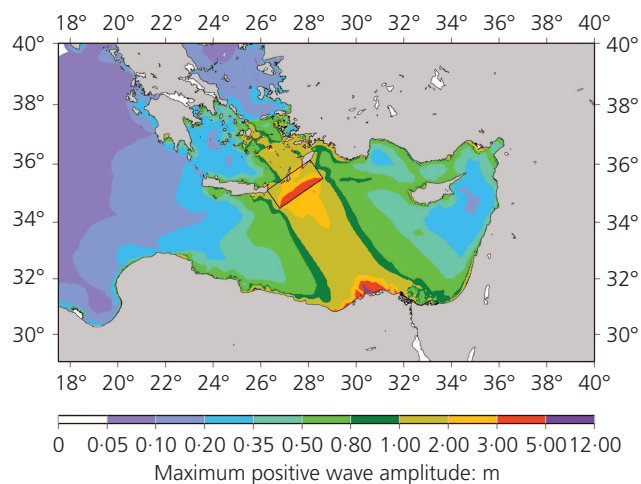


Figure 5. Maximum simulated tsunami amplitude for S2 (uniform-slip $M_w = 8.4$ event located along the eastern Hellenic Arc) in the eastern Mediterranean Sea

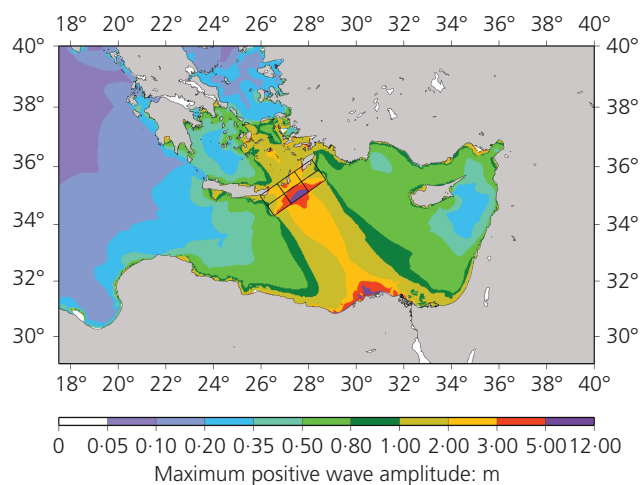


Figure 6. Maximum simulated tsunami amplitude for S3 (variable-slip $M_w = 8.5$ event located along the eastern Hellenic Arc) in the eastern Mediterranean Sea

Libyan and Egyptian coasts. In the case of S2 (eastern Hellenic Arc event with uniform slip and $M_w = 8.4$), the directivity lobe is aimed directly towards the Rosetta promontory of the western Nile Delta near Alexandria, Egypt (Figure 5). Comparison with Figure 6, which shows the simulation results for a variable-slip source (S3) at the same location, shows that the effect of variable slip is concentrated in the near-field; the effect becomes negligible in the far-field along the Egyptian coast, at a distance where the tsunami essentially integrates the seismic source whose details become largely irrelevant to the final wave amplitude. Source S4 features a lobe of directivity aimed at the east Libyan coast and, symmetrically, on the eastern coast of the Gulf of Antalya, Turkey (Figure 7). The effects of irregular bathymetry in the

Offprint provided courtesy of www.icevirtuallibrary.com
Author copy for personal use, not for distribution

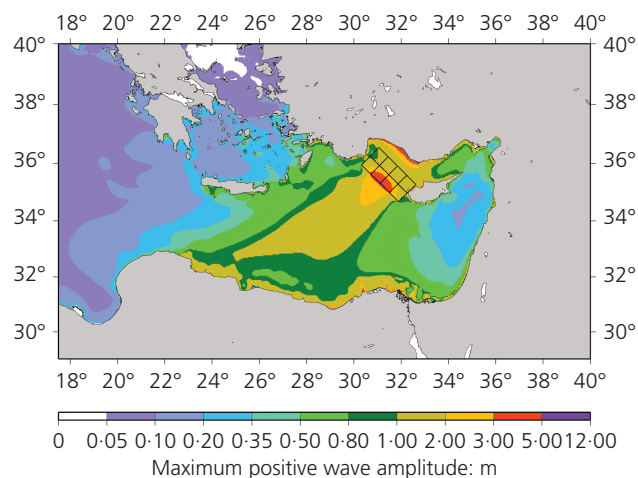


Figure 7. Maximum simulated tsunami amplitude for S4 (plausible $M_w = 8.5$ seismic event located on the NW Cyprian Arc) in the eastern Mediterranean Sea

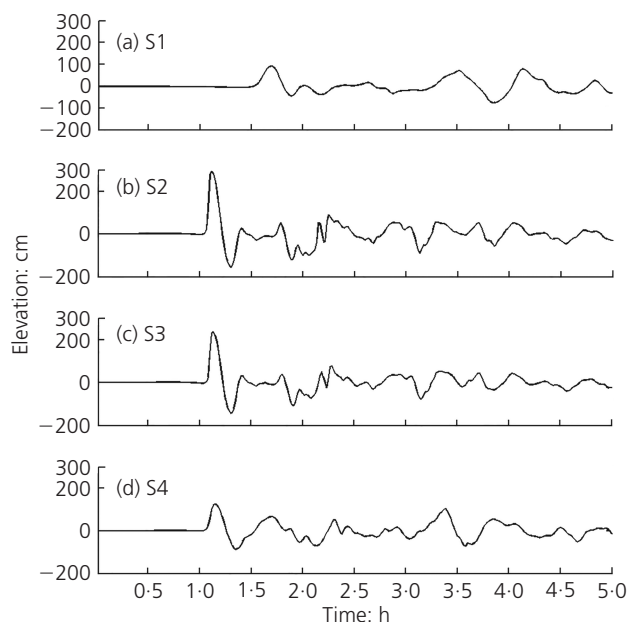


Figure 8. Computed time series of wave elevation for a virtual gauge offshore (20 m depth) of the Rosetta promontory of the western Nile Delta, Egypt (gauge location shown in Figure 2) for four simulated seismic sources. The wave arrives as a leading elevation N-wave

Herodotus Basin and Nile Fan also create a secondary maximum in the vicinity of the Nile Delta.

Detailed results near the Rosetta promontory of the western Nile Delta are presented in Figure 8 in the form of time series of water levels at a virtual gauge located offshore at a depth of 20 m. For S1 (Figure 8(a)), the simulated maximum amplitude is

about 0.9 m (1.4 m peak-to-trough) with a travel time of 90 min. For S2 and S3 (Figures 8(b) and 8(c) respectively), the time series are similar, with maximum amplitudes exceeding 2.0–2.5 m (3.7 and 4.5 m peak-to-peak respectively) with travel times of slightly less than 60 min. Finally, the maximum amplitude under S4 is 1.3 m (2.1 m peak-to-peak) with a travel time of 60 min.

5. Conclusion

Based on reports of documented historical events and seismotectonics of the region under study, plausible megathrust sources ($M_w \geq 8$) were identified in the Hellenic and Cyprian Arcs whose tsunamis would threaten the Egyptian coast near the Rosetta promontory of the Nile Delta. These sources were used in four possible models (three sources along the Hellenic subduction zone and one source on the NW Cyprian Arc) for hydrodynamic simulations with the numerical model Most.

The results indicate that the most significant threat to the area around the Rosetta promontory of the Nile Delta is from a megathrust event along the eastern Hellenic Arc, which could produce zero-to-peak amplitudes at a 20 m offshore gauge of about 3 m. The wave amplitude estimate at the gauge is relatively insensitive to the details of the slip distribution on the fault. Such amplitudes would inevitably lead to structural damage to infrastructure, given that they would be likely further enhanced by runup on dry land. Furthermore, they represent a substantial hazard for Alexandria. In addition, a travel time of 60 min for the initial wave arrival would present a challenge in terms of an orderly evacuation of the threatened coastlines. In addition, and despite a less favourable orientation of their faults, sources in western Crete or along the Cyprian Arc could also result in substantial amplitudes in the western Nile Delta region and near Alexandria (0.9 m and 1.3 m respectively), principally due to refraction by irregular bathymetry in the southeastern Mediterranean Basin.

Acknowledgements

Partial funding for this work was provided by the EU FP7 program Astarte and the Mariolopoulos-Kanagin Foundation. Two of the authors acknowledge fundamental discussions with Professor C. Zerefos and Drs H. Tzalas and T. Repapis.

REFERENCES

- Ambraseys N and Synolakis CE (2010) Tsunami catalogs for the eastern Mediterranean, revisited. *Journal of Earthquake Engineering* **14**(3): 309–330.
- Ammon CJ, Lay T, Kanamori H and Cleveland M (2011) A rupture model of the 2011 off the Pacific coast of Tohoku Earthquake. *Earth, Planets and Space* **63**(7): 693–696.
- Ben-Menahem A and Rosenman M (1972) Amplitude patterns of tsunami waves from submarine earthquakes. *Journal of Geophysical Research* **77**(17): 3097–3128.
- Ebeling CW, Okal EA, Kalligeris N and Synolakis CE (2012) Modern seismological reassessment and tsunami simulation of historical Hellenic Arc earthquakes. *Tectonophysics* **530–531**: 225–239.

Offprint provided courtesy of www.icevirtuallibrary.com
Author copy for personal use, not for distribution

- Flouri ET, Kalligeris N, Alexandrakis G, Kampanis NA and Synolakis CE (2013) Application of a finite difference computational model to the simulation of earthquake generated tsunamis. *Applied Numerical Mathematics* **67**(May): 111–125.
- Fujii Y, Satake K, Sakai S, Shinohara M and Kanazawa T (2011) Tsunami source of the 2011 off the Pacific coast of Tohoku earthquake. *Earth, Planets and Space* **63**(7): 815–820.
- Geller RJ (1976) Scaling relations for earthquake source parameters and magnitudes. *Bulletin of the Seismological Society of America* **66**(5): 1501–1523.
- IOC, IHO and BODC (2003) *Centenary Edition of the GEBCO Digital Atlas*. Published on CD-ROM on behalf of the Intergovernmental Oceanographic Commission and the International Hydrographic Organization as part of the General Bathymetric Chart of the Oceans. British Oceanographic Data Centre, Liverpool, UK.
- Liu PL-F, Yeh H and Synolakis CE (eds) (2008) *Advanced Numerical Models for Simulating Tsunami Waves and Runup (Advances in Coastal and Ocean Engineering, vol. 10)*. World Scientific Publishing, Singapore.
- McClusky S, Balassanian S, Barka A et al. (2000) Global positioning system constraints on plate kinematics and dynamics in the eastern Mediterranean and Caucasus. *Journal of Geophysical Research* **105**(B3): 5695–5719.
- Mitsoudis DA, Flouri ET and Chrysoulakis N et al. (2012) Tsunami hazard in the southeast Aegean Sea. *Coastal Engineering* **60**: 136–148.
- NTHMP (National Tsunami Hazard Mitigation Program) (2012) *Proceedings and Results of the 2011 NTHMP Model Benchmarking Workshop*. US Department of Commerce/NOAA/NTHMP, Boulder, CO, USA, NOAA special report.
- Okada Y (1985) Surface deformation due to shear and tensile faults in a half-space. *Bulletin of the Seismology Society of America* **75**(4): 1135–1154.
- PMEL (Pacific Marine Environmental Laboratory) (2006) *Method of Splitting Tsunami (MOST) User's Manual (Revision 07/06/2006)*. National Oceanic and Atmospheric Administration (NOAA) PMEL, Seattle, WA, USA.
- Pollitz FF, Bürgmann R and Banerjee P (2011) Geodetic slip model of the 2011 M9.0 Tohoku earthquake. *Geophysical Research Letters* **38**(L00G08): 1–6.
- Salamon A, Rockwell T, Ward S, Guidoboni E and Comastri A (2007) Tsunami hazard evaluation of the Eastern Mediterranean: historical analysis and selected modeling. *Bulletin of the Seismological Society of America* **97**(3): 705–724.
- Scholz CH, Aviles CA and Wesnousky SG (1986) Scaling differences between large interplate and intraplate earthquakes. *Bulletin of the Seismological Society of America* **76**(1): 65–70.
- Shaw B and Jackson J (2010) Earthquake mechanisms and active tectonics of the Hellenic Subduction Zone. *Geophysical Journal International* **181**(2): 966–984.
- Shaw B, Ambraseys N, England PC et al. (2008) Eastern Mediterranean tectonics and tsunami hazard inferred from the AD 365 earthquake. *Nature Geoscience* **1**(4): 268–276.
- Subarya C, Chileh M, Prawirodirdjo L et al. (2006) Plate-boundary deformation associated with the great Sumatra–Andaman earthquake. *Nature* **440**: 46–51.
- Synolakis CE (2004) Tsunami and seiche. In *Earthquake Engineering Handbook* (Chen WF and Scawthorn C (eds)). CRC Press, Boca Raton, FL, USA, pp. 9–1–9–90.
- Synolakis CE, Bernard EN, Titov VV, Kânoğlu U and González F (2008) Validation and verification of tsunami numerical models. *Pure and Applied Geophysics* **165**(11–12): 2197–2228.
- Titov VV and González FI (1997) *Implementation and Testing of the Method of Splitting Tsunami (MOST) Model*. Pacific Marine Environmental Laboratory, Seattle, WA, USA, NOAA technical memorandum ERL PMEL-112.
- Titov VV and Synolakis CE (1998) Numerical modeling of tidal wave runup. *Journal of Waterway, Port, Coastal, and Ocean Engineering* **124**(4): 157–171.
- UNU-EHS, EC-JRC and DFUNIBO (United Nations University Institute for Environment and Human Security, European Commission Joint Research Centre and Department of Physics of the University of Bologna) (2009) *Flooding Maps for the Coast of Alexandria, Egypt, One Map and Selected Indicators for Measuring Vulnerability, Scenario Risk Maps for the Town of Alexandria, WP8: Scenarios of Large Tsunami Impact and Risk Assessment and Reduction*. Tsunami Risk and Strategies for the European Region (TRANSFER), Bologna, Italy, Deliverable D8.8.
- Wdowinski S, Ben-Avraham Z, Arvidsson R and Ekström G (2006) Seismotectonics of the Cyprian Arc. *Geophysical Journal International* **164**(1): 176–181.
- Yolsal S, Taymaz T and Yalçiner AC (2007) Understanding tsunamis, potential sources regions and tsunami-prone mechanisms in the eastern Mediterranean. In *The Geodynamics of the Aegean and Anatolia* (Taymaz T, Yılmaz Y and Dilek Y (eds)). Geological Society, London, UK, Special publication 291, pp. 201–230.
-
- WHAT DO YOU THINK?**
To discuss this paper, please email up to 500 words to the editor at journals@ice.org.uk. Your contribution will be forwarded to the author(s) for a reply and, if considered appropriate by the editorial panel, will be published as a discussion in a future issue of the journal.
- Proceedings* journals rely entirely on contributions sent in by civil engineering professionals, academics and students. Papers should be 2000–5000 words long (briefing papers should be 1000–2000 words long), with adequate illustrations and references. You can submit your paper online via www.icevirtuallibrary.com/content/journals, where you will also find detailed author guidelines.